Physical parameters and flows along chromospheric penumbral fibrils

G. Tsiropoula

National Observatory of Athens, Institute of Space Research, Lofos Koufos, 15236 Palea Penteli, Greece (georgia@space.noa.gr)

Abstract. High resolution observations of a sunspot region were obtained on October 3, 1994 with the Multichannel Subtractive Double Pass (MSDP) spectrograph. This instrument installed at the focus of the Vacuum Tower Telescope (VTT) at Tenerife (Canary Islands) operated in the Hα line. Intensity fluctuations and Doppler shift velocities at several wavelengths were derived over a two dimensional field of view. The observed intensity profiles were matched with theoretical ones using a technique proposed by Tsiropoula et al. 1999, which enables the variation of the source function inside the structures and the derivation of some physical parameters like the source function, the Doppler width, the optical depth and the line-of-sight velocity. This technique was applied to the dark fibrils surrounding the sunspot umbra. Once these parameters are estimated several other parameters can be determined like population densities at levels 1, 2, 3 (N_1, N_2, N_3), total particle density of hydrogen, N_H, electron density, N_e, electron temperature, T_e, gas pressure, p, total column mass, m, mass density, ρ, sound speed, c_s etc. Furthermore, using a simple geometrical model we estimated from the line-of-sight velocity the flow velocity along the dark fibrils assuming different sets of inclination angles of the velocity vector with respect to the vertical. We found that there is a flow from the outer edge of the fibrils (in the side of the penumbra), to their inner edge (umbra side), which is consistent to the siphon flow. Moreover, we found a subsonic flow for the entire extent of two of the fibrils considered and for all inclination angle sets, while for one fibril we found a subsonic flow in the outer edge and supersonic velocity in the inner edge for some of the inclination angle sets.

Key words: Sun: chromosphere – Sun: sunspots

1. Introduction

Fibrils constitute the basic elements of the fine structure of active regions. Their relation to other disk features has been discussed by Foukal (1971), who suggested that fibrils are simply the active region analogues of mottles (or spicules) and their differences are mainly due to differences in the geometry and strength of the magnetic field. Moreover, their filamentary appearance is a characteristic aspect of the inhomogeneous character of sunspots penumbrae and superpenumbrae. The arrangement of the fibrils around sunspots is governed by the configuration of the magnetic field and individual fibrils may trace out the actual field lines themselves.

Although there is today a good qualitative description of the morphology and evolution of chromospheric fibrils less work has been done towards the determination of their physical conditions. To our knowledge only Foukal (1971) gives values for some physical parameters (e.g. hydrogen density in the range 5 10^{10} to 2 10^{11} cm^{-3}, temperature greater than 2.5 10^4 and magnetic field greater than 100 G). This is because their derivation encounters a number of intrinsic difficulties because it needs, in the general case, the solution of the 3-D time-dependent non-LTE transfer equations. Nevertheless, as the observation of the shapes and intensities of spectral lines and their interpretation can provide a lot of information about the physical behavior of the different structures and the dynamical processes on the Sun several diagnostic techniques have been attempted that have been proved useful for the derivation of several physical parameters. A lot of work is based on the analysis of the Hα profile. Usually the structures are considered as clouds illuminated by the underlying chromosphere. Furthermore, the source function is assumed to be constant inside them and thus we have to deal with optically thin structures (see e.g. Tsiropoula et al. 1993 and references therein). In a recent work (Tsiropoula et al. 1999) we propose a five-parameter cloud-like fitting "recipe" that assumes a parabolic variation of the source function and permits the modelling of structures no matter if they are optically thin or optically thick including ad-hoc scattering effects. Once this method is applied several physical parameters (like e.g. population densities at levels 1, 2, 3 (N_1, N_2, N_3), total particle density of hydrogen, N_H, electron density, N_e, electron temperature, T_e, gas pressure, p, total column mass, m, mass density and degree of hydrogen ionization can be determined by a method described by Tsiropoula & Schmieder (1997).

Among other physical conditions study of the flow along dark fibrils is also essential because it can add to the understanding of the sunspot penumbrae and the chromospheric Evershed flow. Alissandrakis et al. (1988) found that the flow speed in individual fibrils can be 20 km s^{-1} or more and suggest that it is consistent with the siphon flow model of Meyer & Schmidt (1968). Siphon flows are produced when a pressure difference is

imposed between the footpoints of an arched magnetic flux tube. Different pressure differences produce different flows. Thus, sufficiently small pressure differences produce subsonic flows; in larger pressure differences the flow passes from a subsonic to a supersonic flow close to the apex of the arch and then transits to a subsonic flow through a shock (Maltby 1975; Thomas 1988). Maltby (1997) reviews other mechanisms for this flow, like the wave pressure driven flow and points out that its temporal dependence must be considered.

Another long standing controversy exists on the relation between the Evershed flow and the dark penumbral fibrils. Maltby (1975) e.g. found that the flow is concentrated in channels, while Tsiropoula et al. (1996) found that the axes along $H\alpha \pm 0.3$ Å intensity features are weakly spatially related to the Evershed flow.

From the above it is evident that determination of some physical parameters in individual fibrils, among which flow speeds is crucial. These values can serve, as, at least, initial values in non-LTE models and also can add to our understanding of the Evershed effect at the chromospheric level.

2. Observations

The Multichannel Subtractive Double Pass (MSDP) Spectrograph (Mein 1991) provides sufficient spectral information for relatively broad lines, such as $H\alpha$, and has been used efficiently for studies of chromospheric structures. This instrument records a 2D field of view of a solar region at several wavelengths along the line profile. One of the main advantages of the MSDP spectrograph is that by displacing the entrance slit a large region can be covered quickly in several wavelengths.

The present observations were obtained on October 3, 1994 with the MSDP mounted on the VTT in Tenerife (Canary Islands). Simultaneous observations in 9 wavelengths, 0.3 Å apart in the $H\alpha$ profile of a sunspot region located near the centre of the solar disk (NOAA/AR 7783 at S07 W12) were performed. Twenty consecutive elementary images with small overlapping were recorded every 4 min and were combined by two dimensional cross-correlation techniques to form a single large image of the spot region. The whole region contained 573pixels $\times$ 693pixels covering a field of view of $172'' \times 208''$ (pixel size $0.3''$) with a spatial resolution of about $1''$. Line profiles can be reconstructed using the standard reduction technique for this type of data and Doppler velocities as well as monochromatic intensity images at different wavelengths were computed. From the entire observational sequence which lasted for 1 hour one frame of very good quality obtained at 9:10:14 UT was selected for the present study.

3. Computational method

$H\alpha$ is a very broad absorption line. The wings are formed in the upper photosphere, while the core is formed in the chromosphere. Thus, if one has the possibility to observe the entire line profile then a substantial range of heights of the solar atmosphere can be explored. Various methods have been used in the past for the deduction of different physical parameters of chromospheric structures using this line. A common procedure is their derivation from the comparison between line profiles (e.g. $H\alpha$ profiles) emitted by the body of the structures and those emitted below the structures. This is done from the well-known formula that gives the observed line intensity profile:

$$I_\lambda = I_{0\lambda} e^{-\tau_\lambda} + \int_0^{\tau_\lambda} S_t e^{-t_\lambda} dt_\lambda \tag{1}$$

where $I_{0\lambda}$ is the reference profile emitted by the background atmospheric layer. Usually, an iterative procedure is used and the background profiles are assumed to be the same as those observed in the surrounding chromosphere. Another assumption concerns the variation of the source function inside the structures. The detailed variation of the source function is an unsolved problem. In the case of the classical cloud model (Beckers 1964) it is assumed to be constant and frequency independent. This assumption is valid for optically thin structures. But, in general, it is not realistic to assume that the source function is constant throughout the structure. In this case the variation of the source function with the optical depth must be considered. In a recent work we assume (Tsiropoula et al. 1999) a parabolic variation of the source function with optical depth inside the structure given by:

$$S_t = S_0 (1 + \beta(t - \frac{\tau_0}{2})^2) \tag{2}$$

where S_0 is the source function at the middle of the structure and β the variation factor of the source function. When $\beta > 1$ this variation conforms to the picture given by Gouttebroze et al. (1993), where the source function has its maximum value at the middle of the structure and decreases at both edges. Then the specific intensity in the case of a parabolic variation of the source function is given by:

$$I_\lambda = I_{0\lambda} e^{-\tau_\lambda} + S_0 (1 + \frac{\tau^2 \lambda \beta}{4\phi^2(\lambda)} + \frac{2\beta}{\phi^2(\lambda)})(1 - e^{-\tau_\lambda})$$
$$- \frac{\tau_\lambda \beta S_0}{\phi^2(\lambda)} (1 + e^{-\tau_\lambda}) \tag{3}$$

In the above formulation, $\tau_\lambda = \tau_0 \phi(\lambda)$, where $\phi(\lambda)$ is an approximation to the Voigt profile consisting of the sum of Doppler core and Lorentzian damping wings given by:

$$\phi(\lambda) = e^{-y^2} + \frac{a}{\sqrt{\pi} y^2} \tag{4}$$

where

$$y = \frac{\Delta\lambda - \Delta\lambda_I}{\Delta\lambda_D} \tag{5}$$

$$a = \frac{\Gamma \lambda_0^2}{4\pi c \Delta\lambda_D} \tag{6}$$

In the last relation a is the damping width and Γ the damping constant.

As it has been shown by Tsiropoula et al. (1999) the above method is very relevant to the modelling of chromospheric structures as it assures a good fit between the calculated $H\alpha$ line
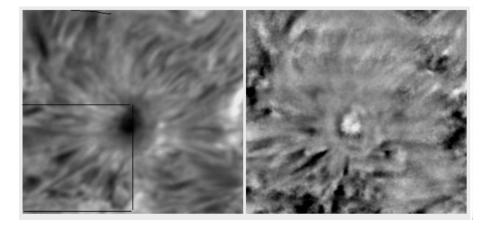
Fig. 1. Intensity (left) and Doppler velocity (right) images of the sunspot region at H$\alpha \pm$ 0.3 Å observed with the MSDP on the VTT in Tenerife on October 3, 1994. The rectangle contains an area of dark fibrils pointing towards the disk centre side

profiles and the observed ones either at line center or in the line wings no matter whether the line is optically thin or optically thick. Furthermore, it provides a relation between the source function and the optical depth which is also derived from 2D non-LTE models (Mein et al. 1996), i.e. a systematic increase of the source function from the top of the structures to their bottom.

Using the above formulation and applying an iterative least-square procedure for non-linear functions we can derive 5 parameters of the chromospheric fibrils. These are: the source function at the middle of the structures, S_0, the variation factor of the source function, α, the optical depth at line centre, τ_0, the Doppler width, $\Delta\lambda_D$ and the Doppler shift, $\Delta\lambda_I$, which yields the line-of-sight component of the mass velocity. This procedure can be applied to the whole region. However, as the results of the fitting are not good for the bright profiles (Tsiropoula et al. 1999) these profiles must be rejected.

Once these parameters are determined the estimation of several other parameters can be made. From the calculated Doppler width values and if we assume a value for the microturbulent velocity, ξ_t, we can deduce the temperature, T_e. From the optical depth at line center, which may be written as:

$$\tau_0 = \frac{\pi^{\frac{1}{2}} e^2}{m_e c} \frac{f\lambda^2}{c} \frac{N_2}{\Delta\lambda_D} d \tag{7}$$

and $\Delta\lambda_D$, N_2, e.g. the number density in the second hydrogen level, can be obtained. Then the electron density, N_e, the total particle density of hydrogen (i.e., neutral plus ionized), N_H and the hydrogen ground-level population, N_1, can be determined from the relations:

$$N_e = 3.2\,10^8\,\sqrt{N_2}\,cm^{-3} \tag{8}$$
$$N_H = 5\,10^8\,10^{0.5\log N_2} \tag{9}$$
$$N_1 = \frac{[N_t - (2+\alpha)N_e]}{1+\alpha} \tag{10}$$

(for details about the derivation of these parameters see Tsiropoula & Schmieder (1997)). Once the above values are determined the derivation of several other parameters is straightforward. Thus the gas pressure, p, the total column mass, m, the mass density, ρ and the isothermal sound speed, c_s, can be determined from the following relations:

$$p = k(N_e + 1.0851 N_H)T_e \tag{11}$$
$$m = (N_H m_H + 0.0851 N_H \times 3.97 m_H)\,d \tag{12}$$
$$\rho = \frac{m}{d} \tag{13}$$

and

$$c_s = \sqrt{RT_e} \tag{14}$$

where d is the path length along the line-of-sight and R the gas constant.

4. Results

The sunspot observed was isolated, nearly axisymmetric with a well developed penumbra showing clearly the Evershed effect. From the whole image constructed from the MSDP profiles a smaller region was selected. It had a size of $69'' \times 59''$ (Fig. 1) and consisted of an apparently well-ordered pattern of fine elongated dark fibrils. Their alignment is roughly radial and suggests magnetic ordering. Their intensity profiles usually have a broad U-shape. They are asymmetrical indicating the presence of substantial mass motions and show a large broadening usually on one wing.

4.1. Physical parameters of dark fibrils

From the processed MSDP profiles and the application of the iterative procedure the 5 parameters have been derived for the entire field of view. The background intensity, $I_{0\lambda}$, was taken as the average of the intensities of bright pixels to take into account the underlying "facular" background. For all parameters 2D maps can be constructed. In Fig. 2 (left) the contour map of the source function is shown (bright profiles have been rejected) in a small area of the entire region containing dark fibrils pointing towards the Sun centre. The source function follows the behavior of the line-centre intensity: it is smaller in the central body of the structures and larger at their edges. In Fig. 2 (right) the contour map of the negative velocities is given, in which velocity channels are clearly apparent. It seems that much of the flow is concentrated in these velocity channels, which occur mostly in parts of the sunspot region occupied by dark fibrils. Usually, these channels are found at the inner legs of the fibrils,
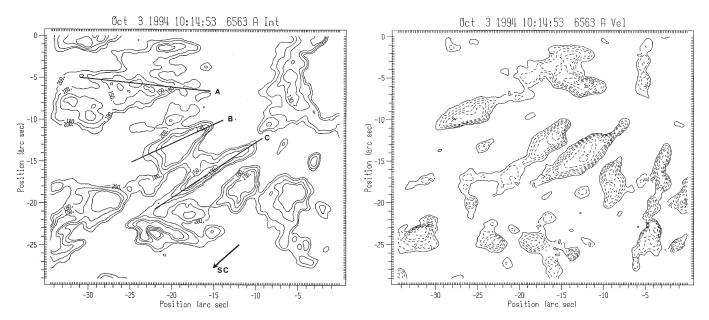
Fig. 2. *Left:* Contour map of the source function. The lines mark the axes of 3 dark fibrils (A, B and C) selected for our analysis. The arrow shows the direction of the disk centre. *Right:* Contour map of the negative velocities representing the flow channels
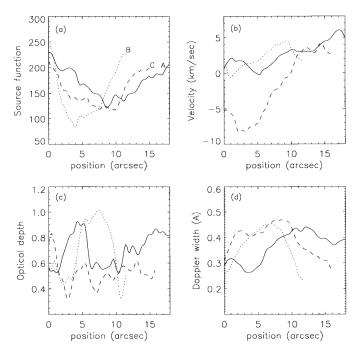

Fig. 3a–d. Variations of the source function **a**, the LOS velocity (positive is towards the observer) **b**, the optical depth at line centre **c** and the Doppler width **d** along the axes of the 3 dark fibrils A, B and C shown in Fig. 2 (left). Position "0″" corresponds to the edge of the structures at the umbra side

at the umbra side and their axes do not coincide with the axes of the dark fibrils in the intensity (or source function) images. More work on this subject is currently in progress (see also Tsiropoula et al. 1996).

Three distinct fibrils A, B and C (Fig. 2 (left)) were selected in order to study the variation of the different parameters along

them. These fibrils are located at the diskward side of the spot and have prominent velocities. In order to follow the variations of the parameters along the central axes of the fibrils, their values were averaged over a strip extending $0.4''$ on either side of the axes while the step along the axis was $0.2''$. Their variations provide a quantitative picture of the observed inhomogeneities. These variations are shown in Figs. 3, 4, 5 and 6 (position "0″" corresponds to the inner part of the structures in the umbra side). Fig. 3a shows the variations of the source function along fibrils A, B and C of Fig. 2 (left). Everywhere along the central axes the source function is smaller than the background intensity at line centre (which is equal to 250), whereas at the two edges it attains the local background (intensities and source functions are given in units of the continuum). In agreement with expectation there are indications of substantial mass motions directed along the fibrils towards the umbra. This can be seen in Fig. 3b where the line-of-sight velocity is shown. It is negative at the inner edges of the fibrils and positive at their outer edge which means that there is a continuous inflow towards the spot consistent with the chromospheric Evershed effect. According to the velocity variations we consider the (chromospheric) edges of the structures to be at the points where the minimum and maximum values of the velocities are attained. Then the projected lengths of the structures can be found. Thus structure A is about 8880 km long, structure B 5900 km and structure C 8510 km. The extreme negative and positive velocity values are -.2 and 6.3 km s^{-1} for fibril A, -.6 and 6.03 km s^{-1} for fibril B and -8.3 and 4.2 km s^{-1} for fibril C, where negative (positive) values denote flows away from (towards) the observer. The optical depth is smaller than ~ 1 (Fig. 3c) almost everywhere for all structures. The optical depth of structure A is smaller along its main body and larger at the two edges, while the inverse is true for fibril B. The optical depth of fibril C is almost constant along it.
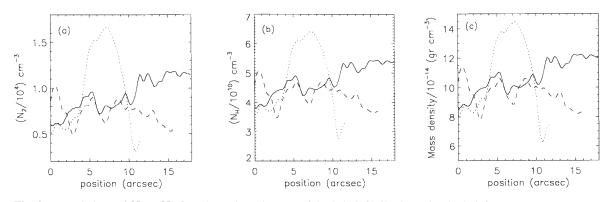
Fig. 4a–c. Variations of N_2 **a**, N_H **b** and ρ **c** along the axes of the 3 dark fibrils shown in Fig. 2 (left)
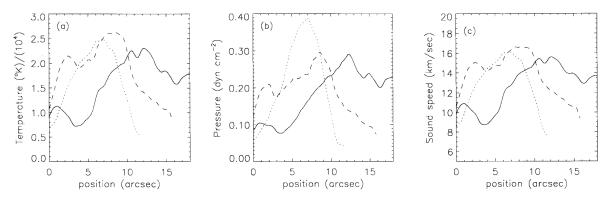

Fig. 5a–c. Variations of the temperature **a**, pressure **b** and sound speed **c** along the axes of the 3 dark fibrils shown in Fig. 2 (left) for $\xi_t = 5\,\mathrm{km\,s^{-1}}$

The Doppler width has values in the range 0.25–0.5 Å (Fig. 3d), which implies rather low temperatures and/or low microturbulent velocities. It is larger along the main body of the structures and decreases towards their two edges.

As physical conditions of fibrils are not given in the literature it is of interest to give estimations of them. Their derivation can be done through the relations (7) to (14) given above. In order to estimate N_2 the path length along the line-of-sight is taken equal to 2000 km. The populations N_2 and N_H and the mass density, ρ, shown in Fig. 4, increase from the outer to the inner edge of fibril A, are larger in the main body and decrease in both edges of fibril B and remain almost constant along fibril C. The variations of the temperature, pressure and sound speed are shown in Figs. 5 and 6. In order to determine the temperature from the Doppler width we have used two values for the microturbulent velocity, (i.e. $\xi_t = 5\,\mathrm{km\,s^{-1}}$ and $\xi_t = 10\,\mathrm{km\,s^{-1}}$). For $\xi_t = 5\,\mathrm{km\,s^{-1}}$ temperatures of the order of 24000 K–25000 K are obtained at the top of the structures, while their pressures are of the order of 0.3–0.4 $\mathrm{dyn\,cm^{-2}}$ and sound speeds of the order of 15–16 $\mathrm{km\,s^{-1}}$. All three parameters have greater values at the body of the structures, and lower values at their two edges. The pressures at the corresponding points where the extreme minimum and maximum velocity values are met are: 0.1–0.22 $\mathrm{dyn\,cm^{-2}}$ for fibril A, 0.08–0.22 $\mathrm{dyn\,cm^{-2}}$ for fibril B and 0.17–0.13 $\mathrm{dyn\,cm^{-2}}$ for fibril C. Thus at the chromospheric level, the inner parts of fibrils A and B have lower pressures than their outer parts, while the inverse is true for fibril C. Larger microturbulent velocity values lead to smaller values of temperature, pressure and sound speed

(e.g. $\xi_t = 10\,\mathrm{km\,s^{-1}}$, lead to smaller values of these parameters at ≈ 0.82 times (Fig. 6)). The mean values and standard deviations of the different physical parameters of the dark fibrils for the whole sunspot region are given in Table 1.

4.2. Flows

The general pattern of the observed line-of-sight (LOS) velocities is consistent with the chromospheric Evershed pattern e.g. redshifts at the diskward side of the spot and blueshifts at the limbward side. This effect can easily be explained in terms of the perspective, i.e. the relation between the flow velocity and its LOS component (Tsiropoula et al. 1996). From the LOS velocities along the 3 fibrils shown in Fig. 3b, which are negative (downflows) at their chromospheric edge towards the umbra and positive (upflows) at the other edge away from the umbra, we can have an idea about the flow along the axes of the fibrils. Thus, apart from the horizontal component, there is in their outer part, an upward component parallel to the LOS, which subsequently decreases, becomes equal to zero at a point along the axis of each fibril and then becomes negative at their inner part towards the umbra. This picture suggests that there is a flow from the outer to the inner part of the fibrils. Of course, the interesting question, if i.e. it is the pressure difference at the footpoints of the structures the driving mechanism of the motion cannot be answered, directly, from the pressure values found by the present computations. This is because the Hα observations represent only the upper (chromospheric) part of the fibrils. What
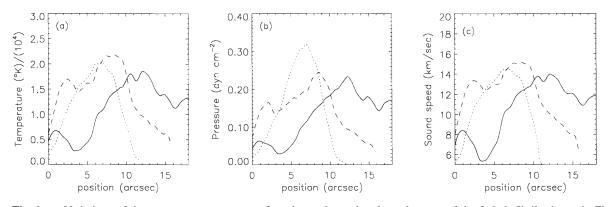
Fig. 6a–c. Variations of the temperature **a**, pressure **b** and sound speed **c** along the axes of the 3 dark fibrils shown in Fig. 2 (left) for $\xi_t = 10\,\mathrm{km\,s^{-1}}$

Table 1. Physical parameters of fibrils

Parameter	Average value	Standard deviation
S	171.1	30.5
τ_o	0.69	0.18
$\Delta\lambda_D$, Å	0.36	0.07
N_1, cm^{-3}	$1.4\ 10^{10}$	$4.0\ 10^9$
N_2, cm^{-3}	$1.1\ 10^4$	$3.7\ 10^3$
N_H cm^{-3}	$4.7\ 10^{10}$	$8.8\ 10^9$
N_e cm^{-3}	$3.1\ 10^{10}$	$5.6\ 10^9$
M, g cm^{-2}	$1.7\ 10^{-5}$	$4.9\ 10^{-6}$
ρ, g cm^{-3}	$8.4\ 10^{-14}$	$2.5\ 10^{-14}$
T, K (for $\xi_t = 5\,\mathrm{km\,s^{-1}}$)	$1.6\ 10^4$	$7.1\ 10^3$
T, K (for $\xi_t = 10\,\mathrm{km\,s^{-1}}$)	$1.1\ 10^4$	$6.9\ 10^3$
p, dyn cm^{-2} (for $\xi_t = 5\,\mathrm{km\,s^{-1}}$)	0.2	0.1
p, dyn cm^{-2} (for $\xi_t = 10\,\mathrm{km\,s^{-1}}$)	0.14	0.1
c_s, km s^{-1} (for $\xi_t = 5\,\mathrm{km\,s^{-1}}$)	12.7	2.9
c_s, km s^{-1} (for $\xi_t = 10\,\mathrm{km\,s^{-1}}$)	10.4	3.7

Fig. 7. Coordinate system for the representation of the flow along the fibrils

happens at their footpoints anchored in the photosphere cannot be derived by the present data. Indirectly, however, we can suggest that because of the lateral pressure balance, the outer footpoints have lower magnetic pressures, as they are embedded in the weaker magnetic field of the penumbra and thus they have higher gas pressures; the inverse is true for the inner footpoints. The flow, therefore, we found from one leg of a structure to the other, driven by a pressure difference, is consistent to the siphon flow.

Knowing only the LOS velocities along the dark fibrils we cannot arrive directly to the values of the flow velocities. This is because the variations of the flow velocities are due, in general, not only to the variations of the LOS velocities along the fibrils, but also to the variations of the inclination angles of the velocity vector with respect to the surface normal and to azimuthal variations. However, by using a simple geometrical model (e.g. Title et al. 1993) and assuming different sets of the inclination angles of the flow velocity vector between the two edges of the structures we can give a picture of the flow velocity variations. The LOS and flow velocity vectors can be described in terms of a rectangular coordinate system OX, OY, OZ centered on the
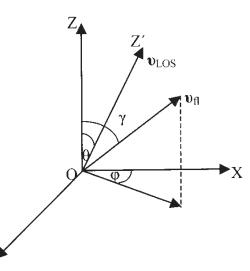
spot centre and rotated with respect to the surface normal OZ$'$ by an angle θ, equal to the heliocentric angle (Fig. 7). For simplicity, we let the LOS velocity vector lie in the plane OX, OZ, which is normal to the solar surface, while the axis OX passes from the spot and Sun centres. The flow speed along the axes of the fibrils has an inclination γ with respect to the surface normal and the flow speed's projection on the solar surface forms an angle ϕ with the axis OX which is measured clockwise ($\phi = 0°$ points to the Sun centre). It is easy to show that the calculated LOS velocity is related to the flow velocity through the relation:

$$v_{LOS} = v_{fl}\left(\sin\theta\ \cos\phi\ sin\gamma + cos\gamma \cos\theta\right) \qquad (15)$$

In our case, the heliocentric angle is equal to 19°, while the azimuth angles can be measured from the filtregrams and are equal to 49° for fibril A, 19° for fibril B and 10° for fibril C. As the inclination angles of the velocity flow vector are not known we adopted different sets of inclinations with respect to the vertical. We started with a value of γ at the outer edge of the fibril and increasing it radially along its axis we get a predefined value of γ for the inner edge. The following sets were used: 30°–60°, 30°–80°, 30°–100°, 40°–60°, 40°–80°, 60°–80° and the results for the fibrils A, B and C are shown in
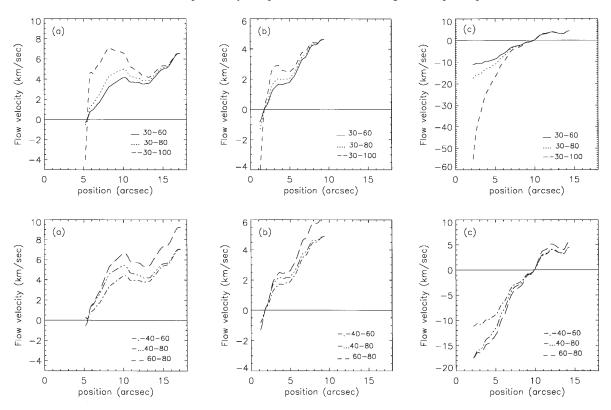
Fig. 8a–c. Variation of the flow velocity for different sets of inclination angles. **a** fibril A, **b** fibril B and **c** fibril C

Fig. 8. The flow is from the outer to the inner edge; positive flow velocities correspond to upflows, while negative velocities correspond to downflows. The behavior of the flow for fibrils A and B is similar. In these two fibrils (Fig. 8a, b) the flow is decelerated from one edge to the other, which can be explained geometrically if the structures are almost horizontal. In fibril C the flow is characterized by a deceleration of the upward moving material, due to the retarding effect of gravity; thereafter the material accelerates as it returns to the surface.

Since the nature of the flow depends critically on the Mach number it is of interest to estimate the latter defined as:

$$M = \frac{|v_{fl}|}{c_s} \tag{16}$$

Thus the flow is always subsonic for the different sets of inclination angles and for the sound velocities calculated either for $\xi_t = 5\,\mathrm{km\,s^{-1}}$ or $\xi_t = 10\,\mathrm{km\,s^{-1}}$ for fibril A and B. For fibril C, on the other hand, the flow is subsonic for the most part of the structure, but it becomes supersonic in the inner edge for the following sets of inclination angles: 30°–80°, 30°–100°, 40°–80°, 60°–80°.

5. Discussion

An important clue to the understanding of the dynamics of the solar atmosphere appears to lie in the knowledge of the physical parameters of the individual structures constituting it. In order to have exact values of these parameters a progress is needed towards 3-D radiative transfer non-LTE modelling. Until then

methods based mainly on the cloud model (Alissandrakis et al. 1990) constitute a significant step towards spectral diagnostics. The method we used in this work enables the variation of the source function with the optical depth, assures a good fit between the calculated Hα line profile and the observed one (Tsiropoula et al. 1999) and seems very appropriate, since it provides reliable estimates of several physical parameters of the chromospheric structures. By using this method we are able to derive, for the first time, values of several physical parameters of the chromospheric fibrils. These values can be used as, at least, first estimates of the physical conditions inside these structures, but also can be used as initial values in non-LTE models (Heinzel 1995). The values derived are, in general, comparable with those derived for the dark mottles (Tsiropoula & Schmieder 1997) with small differences in the mean values leading to the conclusion that the differences between these structures lie mainly in the strength and direction of the magnetic field. Several points about the uncertainties concerning the derivation of the parameters and the reliability of the method used in this work have already been discussed by Tsiropoula & Schmieder 1997 and Tsiropoula et al. 1999. A point of uncertainty related to the subsonic or supersonic character of the flow will be discussed in the next paragraph.

Among other parameters determination of the flow velocities along chromospheric fibrils is of high importance for the understanding of the sunspot penumbrae. A fundamental difficulty in this determination lies, however, in the fact that the only parameter we have available is the LOS velocity. Nevertheless, we can estimate the flow velocities by using a simple geomet-

rical configuration and assuming different inclination angles of the velocity vector with respect to the surface normal. Our results picture a unidirectional flow from the edge of the fibrils at the penumbra side towards the edge at the umbra side. In two of the fibrils (A and B) the flow velocity is upwards and it is decelerated from the outer to the inner edge being always subsonic for all sets of the inclination angles considered. In fibril C the ascending material at the outer edge has subsonic velocities and it is decelerated, while the descending material is accelerated attaining supersonic velocities at its inner edge for almost all of the inclination angle sets considered. As the subsonic or supersonic character of the flow depends on the ratio of the flow velocity to the sound speed it is of interest to examine the uncertainties introduced in their calculations. It has been proven, already, that of all the parameters calculated by the classical cloud model, the differential cloud or the cloud model with non-constant source function, the velocity is the most model-independent parameter (Alissandrakis et al. 1990, Tsiropoula et al. 1999). On the other hand, the value of the microturbulent velocity, ξ_t is crucial in the determination of the sound speed. As the range of the values of ξ_t is not *a priori* known it can be obtained indirectly by considering if the obtained values of T and p are reasonable. Due to the relatively small Doppler widths large values of ξ_t would lead to too low values of T and p. We consider that a reasonable range for ξ_t is between 5 km s^{-1}–15 km s^{-1}. By using this range for ξ_t the subsonic or supersonic character of the flow is retained.

The kind of flow found is consistent to the siphon flow, i.e. upflow in the higher gas pressure (lower magnetic pressure) footpoint, and downflow in the lower gas pressure (higher magnetic pressure) Furthermore, according to Maltby (1975), subsonic flows are produced by small pressure differences between the footpoints of the flux tubes, while large pressure differences produce subsonic flows in the outer, larger pressure footpoint, which are accelerated and transit to supersonic at the top of the structures passing again to subsonic near the inner footpoint through a compression shock. footpoint. We can, therefore, suggest that in two of the fibrils (A and B) there must exist small pressure differences, while in fibril C a large pressure difference must exist.

A main discrepancy between our results and the siphon flow models of Maltby (1975) or Thomas (1988) lies in that for two of the fibrils having subsonic flows (i.e. A and B) we found a flow which is decelerated from the outer to the inner edge (the models predict an acceleration), while for fibril C the flow is characterized by a deceleration of the upward moving material, and an acceleration as it returns to the surface (the models predict an acceleration and a deceleration respectively). We can state some reasons for these discrepancies. It should be emphasized that the siphon flow models assume a steady flow along the flux tubes. On the other hand, our results provide a picture of the flow only at one particular time. The flow along fibrils, however, is time dependent, showing a quasi-periodic behavior with periods of 10–15 min (Tsiropoula et al. 1997). This behavior has to be explained by a dynamical, and not stationary, siphon flow model or probably by other mechanisms based on waves or convective motions, which are not so far sufficiently analyzed.

Finally, we would like to notice, that after a first inspection of the whole time series the downflows at the inner edges of the fibrils end at larger patches of downflows which can be identified as the well-known velocity flow channels and which seem to carry the Evershed flow. We provide a contour map of negative velocities showing clearly the existence of flow channels the axes of which do not coincide with the axes of the dark fibrils in the intensity images. It is also evident that systematic downflows are persistent in the footpoints of the fibrils at the umbra side during the whole time series. Then when and how is the material supplied? What is the real evolution of the flow as time proceeds? And which is the relation between the flows along dark fibrils and the Evershed flow? In order to answer these questions observations of the present quality but with better temporal resolution are needed.

References

Alissandrakis C.E., Dialetis D., Mein P., et al., 1988, A&A 201, 339

Alissandrakis C. E., Tsiropoula G., Mein P., 1990, A&A 230, 200

Beckers J.M., 1964, Ph.D. Thesis, Utrecht

Foukal P., 1971, Solar Phys. 20, 298

Gouttebroze P., Heinzel P., Vial J.-C., 1993, A&A 99, 513

Heinzel P., 1995, A&A 299, 563

Maltby P., 1975, Solar Phys. 43, 91

Maltby P., 1997, In: Schmieder B., del Toro Iniesta J.C., Vazquez M. (eds.) Advances in the Physics of Sunspots. ASP Conf. Ser. vol. 118, 91

Mein N., Mein P., Heinzel P., et al., 1996, A&A 309, 275

Mein P., 1991, A&A 248, 669

Meyer F., Schmidt H.U., 1968, Z. Angew. Math. Mech. 48, 218

Thomas J.H., 1988, ApJ 333, 407

Title A.M. Frank Z.A., Shine R.A., et al., 1993, ApJ 403, 780

Tsiropoula G., Alissandrakis C.E., Schmieder B., 1993, A&A 271, 574

Tsiropoula G., Alissandrakis C.E., Dialetis D., et al., 1996, Solar Phys. 167, 79

Tsiropoula G., Schmieder B., 1997, A&A 324, 1183

Tsiropoula G., Dialetis D., Alissandrakis C.E., et al., 1997, Solar Phys. 172, 139

Tsiropoula G., Madi C., Schmieder B., 1999, Solar Phys. 187, 11